Journal of Materials Chemistry B

Accepted Manuscript

ROYAL SOCIETY OF CHEMISTRY

www.rsc.org/materialsB

Cite this: DOI: 10.1039/c0xx00000x

www.rsc.org/xxxxxx

ARTICLE TYPE

A novel strategy for the aqueous synthesis of down-/up-conversion nanocomposites for dual-modal cell imaging and drug delivery†

Peng Zhao,[a] Jing Zhang,[b] Yihua Zhu,[a]* Xiaoling Yang,[a] Xin Jiang,[a] Yuan Yuan,[b] Changsheng Liu[b] and Chunzhong Li[a]*

Received (in XXX, XXX) Xth XXXXXXXXX 20XX, Accepted Xth XXXXXXXXX 20XX
DOI: 10.1039/b000000x

A highly efficient multifunctional nanoplatform for dual-modal luminescence imaging and pH-responsive drug delivery has been developed on the basis of a facile and novel strategy by covalently binding up-conversion (UC) luminescence $NaYF_4$:Yb,Er nanoparticles with down-conversion (DC) fluorescence $AgInS_2$-ZnS quantum dots. Due to the enriched carboxylic groups in the polymer shell of UC nanoparticles, the as-prepared nanocomposites (NCs) are water-soluble, functionalizable and enable to load anti-cancer drug molecules, doxorubicin (DOX), by simple physical adsorption. The release of DOX from NCs was controlled by varying pH, with an increased drug dissociation rate in acidic environment, favorable for controlled drug release. Moreover, the endocytosis and the efficient drug release properties of the system were confirmed by luminescence microscopy. Hence, this approach provides a valuable method for fabricating a NC system with highly integrated functionalities for dual-modal luminescence cell imaging and targeted cancer therapy.

1. Introduction

Fluorescence semiconductor quantum dots (QDs) have been systematically investigated over the last three decades because of their unusual optical and electronic properties that are tunable with size and composition.[1-3] Recently, ternary I-III-VI semiconductors and their alloys are among the most suitable alternatives to Cd- and Pb-based traditional semiconductors because of their outstanding light-emitting properties as well as their low toxicity, and have shown great promise in biolabelling and bioimaging applications.[4-8] However, autofluorescence often causes false positive results while mono-fluorescence QDs and UV-vis excitation are used. An alternative way to overcome this drawback can be the utilization of up-conversion nanoparticles (UCNPs). By using near-infrared (NIR) light as the excitation source, UCNPs have many unique advantages including low autofluorescence, resistance to photobleaching and deep penetration length in biological tissues without causing any significant tissue damage.[9-11] Therefore, combining these two kinds of luminescent NPs into a nanocomposite (NC) label is extremely desirable for down- and up-conversion (DC and UC) dual-modal imaging applications, which will greatly improve the detection veracity and decrease the false positive results as well.

To date, multifunctional NCs have played an increasingly important part in a various range of applications, such as drug delivery, multimodal imaging, diagnosis and therapy, and so on.[12-17] Among the multifunctional NCs, DC-UC NCs are particularly desirable in biomedical fields for dual-modal luminescence imaging.[13,18,19] Chen and co-workers had achieved DC-UC dual-mode luminescence from Eu^{3+} ions in $NaGdF_4$ NCs that consist of the $NaGdF_4$:Yb,Tm core and the $NaGdF_4$:Eu shell, but it generally would not be easy to obtain simultaneously strong DC and UC luminescence by this doping method, which could be attributed to the energy level mismatch between dopants and hosts.[18] Li and co-workers fabricated binary nanostructures with dual-mode luminescence properties through ultrasonic method, nevertheless, the NCs synthesized by the liquid-solid-solution process are easy to detach from the particle surface in organic solvents, resulting in decomposition of the NCs.[19] More recently, Wang and co-workers have embedded QDs and UCNPs into polymer matrixes through polymerization, but it is inevitable to aggregation during polymerization.[13] Therefore, it remains a challenge to fabricate DC-UC luminescent NCs with strong DC and UC emission, stable composition, high water stability, good biocompatibility and satisfactory bioconjugatability.

Herein, we rationally designed a novel and well-defined NC for dual-modal imaging and drug delivery *via* covalently linking water-soluble QDs and UCNPs. Highly emissive and amino-modified $AgInS_2$-ZnS (ZAIS) QDs have been successfully synthesized directly in aqueous media, then bonded with carboxyl-functionalized $NaYF_4$:Yb,Er NPs, as shown in Fig. 1. The obtained UCNPs/ZAIS NCs can emit yellow fluorescence (ZAIS, DC) and green luminescence ($NaYF_4$:Yb,Er, UC) *via* irradiation with UV (365 nm) and NIR (980 nm) light, respectively. With the help of N-hydroxysuccinimide (NHS) and 1-ethyl-3-(3-dimethylaminopropyl)carbodiimide hydrochloride (EDC), the NCs were then labeled with folic acid (FA) by the formation of amide bonds between amine group in the FA and carboxyl groups in UCNPs. In addition, the experimental results demonstrated that the abundant carboxyl groups of poly(acrylic

acid) (PAA) on the surface of NCs enabled the carriers to load a large amount of doxorubicin (DOX). Finally, these FA-functionalized NCs are capable of application for DC-UC dual-modal luminescence imaging and pH-responsive controlled drug release in cancer cells.

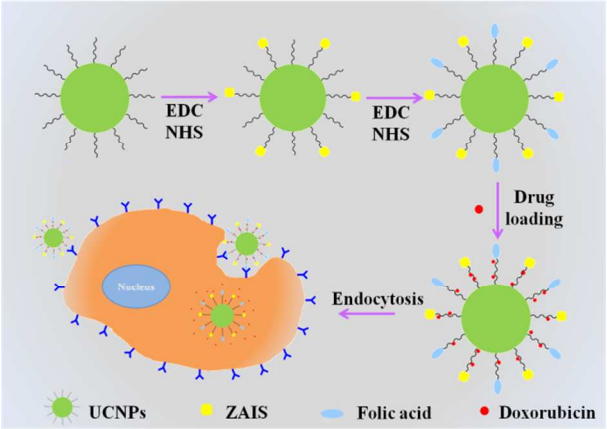

Fig. 1 Schematic of the synthesis of DOX-UCNPs/ZAIS NCs and folate-mediated binding of tumor cells with folate receptor expression.

2. Experimental

2.1 Materials.

$RE(NO)_3$ (99.9%) (RE = Y, Yb, Er), and PAA, indium(III) acetate (99.99%), 2-mercaptoethylamine hydrochloride (98%), EDC, NHS, 2-(-N-morpholino)ethanesulfonic acid (MES), FA, DOX were obtained from Alfa Aesar Co. Ltd., Silver(I) nitrate (99.9%), zinc(II) nitrate (99%), sodium citrate (99%), sodium sulfide, tris(hydroxymethyl) methanamine (Tris), 3-[4,5-dimethylthialzol-2-yl]-2,5-diphenyltetrazolium bromide (MTT) were purchased from Sigma-Aldrich Chemicals Co., all other chemicals were purchased from the Shanghai Chemical Reagent Co.. All chemicals were used as received. Ultrapure water (18 MΩ cm^{-1}) was used for all experiments

2.2 Synthesis of carboxyl-modified β-$NaYF_4$:Yb,Er UCNPs.

Carboxyl-modified $NaYF_4$:Yb,Er UCNPs were prepared as the method we reported before.[20,21] Typically, 1.2 mmol of $RE(NO_3)_3$ (Y : Yb : Er = 80 : 18 : 2), 2.4 mmol of NaCl and 0.6 g of PAA were dissolved in 20 mL ethylene glycol (EG) and mixed thoroughly to form a transparent solution. Then NH_4F (5 mmol) dissolved in 15 mL EG was added to the above mixture under stirring. The resulting mixture was transferred into a 50 mL Teflon-linked autoclave. The autoclave was then sealed and heated to 200 °C for 12 h. After cooling down to room temperature, the products were collected by centrifugation, washed with ethanol and distilled water several times, and dried in an oven at 60 °C.

2.3 Synthesis of amino-functionalized ZAIS QDs.

In a typical synthesis, a 100 mL aqueous solution containing 0.1 mmol $AgNO_3$, 0.4 mmol $In(NO_3)_3$, 0.5 mmol 2-mercaptoethylamine hydrochloride and 0.1 mmol glutathione was prepared in a 250 mL three-necked flask. Under vigorous stirring, 3 mL of 0.2 M Na_2S (0.6 mmol) solution was injected. The resulting mixture was heated to 100 ºC, and was maintained at this temperature for 10 min to allow growth of $AgInS_2$ QDs. Then, an 8 mL aqueous solution containing 0.8 mmol $Zn(NO_3)_2$ and 1 mmol sodium citrate was slowly added into the mixture. This was followed by dropwise addition of 2 mL of 0.2 M Na_2S solution (0.4 mmol). The last two steps took about 10 min. The reaction mixture was further heated for 2 h at 100 ºC. The solution was concentrated to 20 mL with a rotary evaporator, and a minimal amount of 2-propanol was added to precipitate the resulting QDs, which were redispersed in a minimal amount of water. Excess salts were completely removed by repeating this procedure two times. The purified QDs were vacuum-dried to a powder form or resuspended in water for further use.

The quantum yield (QY) tests were carried out and the QY was calculated according to eqn (1):[22]

$$QY = Q_R \times (A_R/A) \times (F/F_R) \times (\eta/\eta_R)^2 \quad (1)$$

Herein, the F is the area of the measured emission spectrum, η is the refractive index, and A is the UV-vis absorbance of the luminescent solution. The subscript R refers to the reference fluorophore with a known quantum yield. In this work, Rhodamine B was chosen as the reference and the absorption and excitation wavelength was set at 340 nm.

2.4 Fabrication of UCNPs/ZAIS NCs.

Briefly, EDC (2 mM) and NHS (5 mM) were firstly added to 10 mL of MES buffer (10 mM, pH 5.5) containing 50 mg UCNPs to activate the surface carboxylic acid group. The mixture was incubated at room temperature for 2 h with shaking. After centrifugation and washed with water for three times, the precipitate was added to 20 mL of ZAIS solution (1 mg mL^{-1}). The linkage reaction was allowed to proceed at 30 ºC for 4 h. Afterwards, 50 mg Tris was added to block any unreacted NHS. Finally, the obtained NCs were centrifuged, washed several times with water.

2.5 Bioconjugation of UCNPs/ZAIS NCs with FA (UCNPs/ZAIS-FA).

EDC (2 mM) and NHS (5 mM) were firstly added to 5 mL of MES buffer (10 mM, pH 5.5) containing 5 mL of NCs (2 mg mL^{-1}), the mixture was incubated at room temperature for 2 h with shaking. After centrifugation and washed with water for three times, the precipitate was added to 10 mL of FA solution (5 mg mL^{-1}), and the mixture was kept incubating at room temperature for 4 h. Afterwards, 50 mg Tris was added to block any unreacted NHS. Finally, the resulting NCs were collected by centrifugation, washed with water three times, redispersed in 5 mL of phosphate buffer, and stored in the dark at 4 ºC for further application.

2.6 *In vitro* DOX loading and control release.

DOX loading onto NCs (DOX-UCNPs/ZAIS) was done by soaking 50 mg of UNCPs/ZAIS NCs in a 5 mL solution of DOX in phosphate buffer solution (PBS, pH = 7.4) for 24 h at room temperature. For the DOX loading saturation experiment, 20 mg of UCNPs/ZAIS was soaked in 5 mL of DOX solution with different concentrations (50 - 300 mM) for 24 h at room temperature. Free DOX was removed by centrifugation and washed three times with PBS buffer. To evaluate the DOX loading amount, the supernatant was collected, and the residual DOX content was determined using the calibration curve of DOX standard solution by the UV-vis measurement at 480 nm.

To measure *in vitro* drug release, the DOX-UCNPs/ZAIS NCs were immersed in 5 mL of PBS buffer solutions (pH 7.4 and 5.0) at room temperature with gentle shaking. At predetermined time intervals, 4 mL of the released medium was taken out to determine the released drug concentration and then returned to the original release medium. The amount of released DOX was measured by UV-vis spectrophotometer at 480 nm.

2.7 Cytotoxicity assays of UCNPs/ZAIS-FA NCs.

MTT assays were carried out to evaluate the potential cytotoxicity of UCNPs/ZAIS-FA NCs in HeLa cells (human cervical carcinoma cells). HeLa cells were plated out in 96-well plates at a density of 3000 cells per well and incubated 24 at 37 ºC in a humidified atmosphere of 5% CO_2 to allow the cells to attach and grow. The UCNPs/ZAIS-FA NCs were sterilized by autoclaving, and then serial concentrations of the NCs were added and incubated for 24 h and 48 h in 5% CO_2 at 37 ºC. Then 20 µL of MTT solution (5 mg mL^{-1}) was added to each well containing different amouts of UCNPs/ZAIS-FA NCs and incubated at 37 ºC for 4 h. The medium and MTT were then removed, and the MTT-formazan crystals were dissolved in 150 µL of DMSO, and placed on a shaking table, 150 rpm for 5 minutes, to thoroughly mix the formazan into the solvent. The absorbance of the suspension was recorded under a microplate reader at 490 nm.

2.8 *In vitro* cytotoxicity assays of DOX-UCNPs/ZAIS-FA NCs.

For DOX drug delivery experiment, HeLa cells were incubated with series concentrations of free DOX, UCNPs/ZAIS-FA and DOX-UCNPs/ZAIS-FA for 1 h and then changed to fresh medium after washing. After further 24 h incubation, the cell viability test was carried out by MTT assay.

2.9 Cellular uptake.

Cellular uptake was examined using confocal laser scanning microscopy (CLSM) against HeLa cells. The HeLa cells were seeded in 6-well culture plates (a clean cover slip was put in each well) and grown overnight as a monolayer, then were incubated with UCNPs/ZAIS-FA and DOX-UCNPs/ZAIS-FA at 37 °C for 1 h. Thereafter, the cells were rinsed with PBS three times, fixed with 2.5% formaldehyde at 37 °C for 10 min, and then rinsed with PBS three times again. For nucleus labelling, fixed cells were incubated with DAPI. The cells treated with NCs were subjected to a CLSM equipped with NIR 980 nm diode laser for observation.

2.10 Characterization.

To demonstrate the overall uniformity and morphology of the particles, the samples were characterized by scanning electron microscopy (SEM) using JEOL SM-6360LV microscope equipped with an energy dispersive X-ray spectroscopy (EDS). ICP-AES (optima 7300DV, Perkin-Elmer) was used to measure the concentrations of Ag and In elements in the samples. Transmission electron microscopy (TEM) images were taken with a JEOL 2011 microscope (Japan) operated at 200 kV. The crystal structure was investigated by X-ray power diffraction (RIGAK, D/MAX 2550 VB/PC, Japan). Fluorescence spectra were measured on a Fluorolog-3-P UV-vis-NIR fluorescence spectrophotometer (Jobin Yvon, France), with a CW NIR laser at λ = 980 nm as the excitation source. The Fourier transform infrared (FTIR) spectra were recorded on a Nicolet 5700 Fourier transform infrared spectrometer within the range of 500 - 4000 cm^{-1}. CLSM images were observed by confocal laser scanning microscope (Olympus, FV 1000).

3. Results and discussion

As shown in SEM image (Fig. 2a), the as-obtained $NaYF_4$:Yb,Er NPs were highly monodisperse with a mean particle size of 150 nm. The obvious lattice fringes in the HRTEM image (Fig. S1, ESI†) confirm the high crystallinity. The interplanar distances between adjacent lattice planes (0.30 nm) is well coincident with the (110) plane of $NaYF_4$:Yb,Er. The hexagonal phase structure of the UCNPs is identified by the selected area electron diffraction pattern (Fig. S1, inset, ESI†), which shows the spotty polycrystalline diffraction rings corresponding to the specific (100), (210) planes of the hexagonal $NaYF_4$:Yb,Er lattice.[23] Fig. 2b presents the TEM image of ZAIS QDs, it can be seen that the nanocrystals were dispersed very well and no particle aggregations were formed. The average size of the nanocrystals was ~2 nm. The HRTEM image (Fig. 2b, inset) displays lattice fringes for the nanocrystals, indicating that these QDs exhibit high crystallinity. After covalently linking, it is observed from Fig. 2c that ZAIS QDs were successfully attached to the surface of UCNPs and no aggregation was observed. In the EDS spectrum (Fig. 2d), beside the peaks of UCNPs (Na, Y, F, Yb), Ag, In, S, and Zn elements were also detected. TEM examination of a selected area of the UCNPs/ZAIS nanocomposites combined with the corresponding EDS mapping are presented in Fig. S2 (ESI†). The mapping profile for the elements of F, Na, Y, Zn and In demonstrate the homogenerous distribution of ZAIS throughout the NCs.

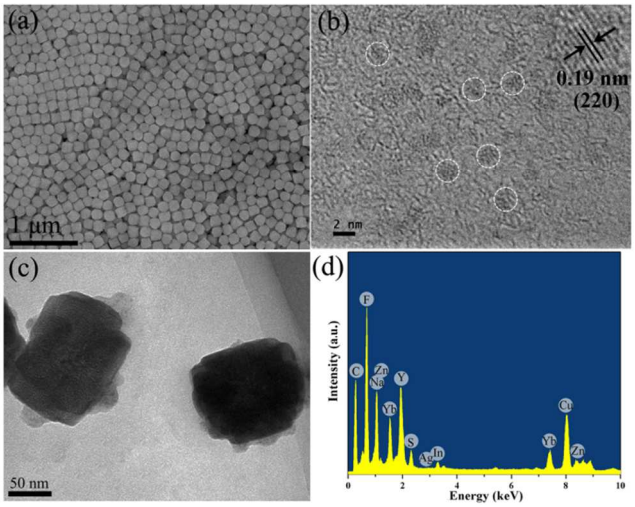

Fig. 2 (a) SEM image of β-$NaYF_4$:Yb,Er UCNPs. (b) TEM image of obtained ZAIS QDs. Inset: HRTEM image of a single ZAIS QDs. (c) TEM image of UCNPs/ZAIS NCs. (d) EDS spectrum of UCNPs/ZAIS NCs.

From the XRD patterns shown in Fig. 3a, the characteristic diffraction peaks matched well with tetragonal chalcopyrite crystal structure ZAIS (JCPDS 85-1575)[24] and hexagonal phase of $NaYF_4$:Yb,Er (JCPDS 28-1192),[25,26] the XRD pattern of the

UCNPs/ZAIS NCs display nearly the same pattern as pure UCNPs with a tiny diffraction peak at 2θ = 28°, which can be index as (112) plane of ZAIS, suggesting the coexistence of ZAIS and $NaYF_4$:Yb,Er NPs in the NCs. The successful attachment of QDs to the surface of UCNPs can be established through FTIR spectra and the specific recognition of carboxyl-modified $NaYF_4$:Yb,Er NPs before and after ZAIS coupling (Fig. 3b). For the carboxyl-capped UCNPs, weak IR peaks at 1469, 1644, 2925 and 2852 cm^{-1} are attributed to the asymmetric and symmetric stretching vibrations of the carboxylic group and the C-H bond, respectively;[27,28] after coupling, strong IR band centered at 1400 and 1630 cm^{-1} were observed, which can be attributed to the stretching vibrations of the C-N bond and the N-H bending mode of amino group ($-NH_2$).[29] These features verify the successful binding of ZAIS with UCNPs.

Both the DC and UC emission spectra of the $NaYF_4$:Yb,Er NPs and ZAIS QDs before and after the fabrication of the NCs were recorded, and are shown in Fig. 3c. The spectra demonstrated that the DC emission of the QDs and the UC emission of the UCNPs were quenched slightly after attachment. In other words, the optical properties of the QDs and UCNPs were well maintained in the NCs. The green (525, 550 nm) and red (665 nm) UC luminescence of $NaYF_4$:Yb,Er nanocrystals can be assigned to $^2H_{11/2} \rightarrow {}^4I_{15/2}$, $^4S_{3/2} \rightarrow {}^4I_{15/2}$ and $^4F_{9/2} \rightarrow {}^4I_{15/2}$ transition, respectively.[30-32] It is well-known for ternary semiconductors that fluorescence emission mostly comes from transitions between states of donor-acceptor pairs induced by defects in the NCs such as chalcogenide vacancies, silver vacancies, chalcogenide interstitials, etc.[33] By fix the Ag : In molar ratio of 0.25 : 1 in our ZAIS QDs, which was confirmed by ICP-AES, the bright yellow fluorescence (590 nm) was observed

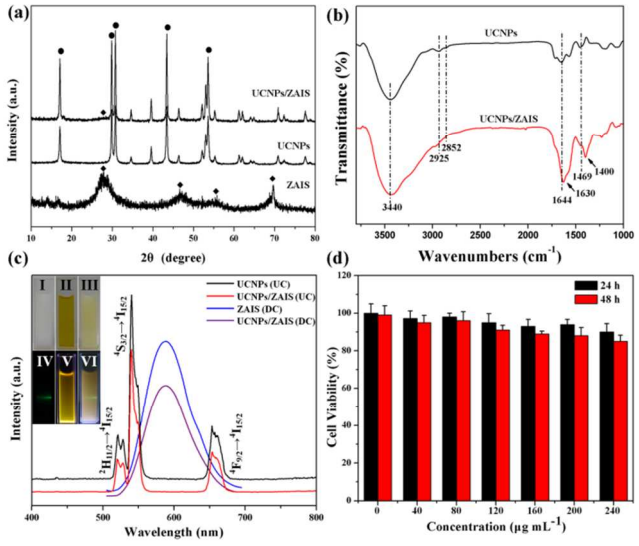

Fig. 3 (a)The wide-angle XRD patterns of $NaYF_4$:Yb,Er UCNPs, ZAIS QDs and UCNPs/ZAIS NCs. (b) FTIR spectra of UCNPs (black curve) and UCNPs/ZAIS NCs (red curve). (c) Luminescence DC and UC spectra before and after the fabrication of NCs. Inset: daylight (top) and luminescence (bottom) photographs of the corresponding samples dispersed in water; I, IV: UCNPs; II, V: ZAIS QDs; III, VI: UCNPs/ZAIS NCs. (d) Cell viability test in HeLa cell lines cultured with UCNPs/ZAIS NCs at different concentrations at 37 °C for 24 and 48 h.

under excitation of 365 nm, with a QY of 18%.[34] As shown in Fig. 3c inset (VI), the dual-modal luminescent UCNPs/ZAIS NCs can emit yellow DC fluorescence of ZAIS QDs and green UC luminescence of $NaYF_4$:Yb,Er NPs under UV (365 nm) and NIR (980 nm) irradiation, respectively.

The cytotoxicity evaluation of the obtained UCNPs/ZAIS NCs were carried out with the MTT assay. As can be seen from Fig. 3d, more than 90% and 85% HeLa cells cultured with UCNPs/ZAIS NCs remained viable even when the NC concentration was up to 240 μg mL^{-1} after incubation for 24 h and 48 h, respectively. Therefore, when the concentration of NCs was 80 μg mL^{-1} that was used for cell imaging later, over 95% of the cells were alive for both 24 and 48 h, suggesting a good biocompatability.

We next studied the drug delivery property of the NCs. UCNPs prepared by our method have a PAA shell with a great deal of carboxyl groups in the outer layer, which makes them have good water-solubility and biocompatibility. Even after amino-modified ZAIS QDs attachment, lots of carboxyl groups in the outer layer still exist, which was further confirmed by zeta-potential (-27 mV) and FTIR (Fig. 3b, red curve). DOX, a commonly used anti-cancer drug, was used as the model molecule in this work. The preliminary test demonstrates that DOX is able to load onto t UCNPs/ZAIS NCs. Reddish precipitate and nearly colorless supernatants were observed after centrifugation of the DOX-UCNPs/ZAIS mixtures, indicating DOX binding on UCNPs/ZAIS which were pulled down by the centrifugation force (Fig. S3, ESI†).[35]

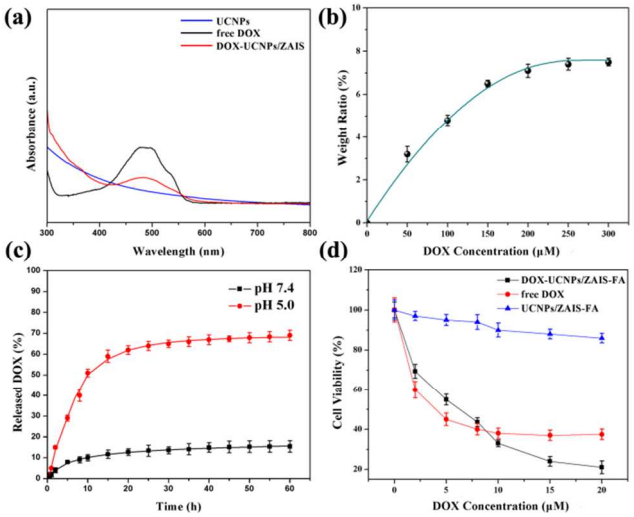

Fig. 4 (a) UV-vis absorbance spectra of free DOX, bare UCNPs, and DOX-UCNPs/ZAIS solutions. (b) Quantification of DOX loading at different DOX concentrations in PBS (pH 7.4). (c) Real time monitoring DOX release from DOX-UCNPs/ZAIS NCs in PBS at two different pH values. (d) Concentration-dependent cell viability of HeLa cells treated with free DOX, UCNPs/ZAIS-FA and DOX-UCNPs/ZAIS-FA.

For DOX loading into the NCs, UCNPs/ZAIS solutions were added with different amounts of DOX for drug encapsulation and composite preparation. It was measured that the DOX loading capacity increased with the increasing amounts of added DOX, showing the saturated maximal DOX loading efficiency was 7.5% (w/w) (Fig. 4b), determined by the characteristic DOX absorption peak at 480 nm (Fig. 4a). The DC-UC luminescence spectra of UCNPs/ZAIS and DOX-UCNPs/ZAIS were also measured using UV and 980 nm laser as the excitation light, respectively (Fig. S4,

ESI†). The UC emission band from 500 to 560 nm had a significant decrease, while the UC emission band at 650 nm was essentially unchanged in the DOX-UCNPs/ZAIS sample compared to bare UCNPs/ZAIS without loading DOX. The change in the spectra are attributed to the resonance energy transfer from UCNPs/ZAIS to DOX. (DOX absorption peak overlaps with the green emission of UCNPs), further evidencing the binding of DOX on UCNPs/ZAIS. Meanwhile, the DC emission spectrum displays a typical fluorescence spectrum of DOX after DOX loading. The *in vitro* release of DOX from the DOX-UCNPs/ZAIS NCs could be controlled by changing pH values. In neutral PBS (pH 7.4) to simulate normal physiological conditions, DOX was released from the samples in a very slow speed and the cumulative release of DOX was only about 15.4% within 60 h. However, in PBS at pH 5.0 to simulate the intracellular conditions of cancer cells, the release rate of DOX became much faster and the cumulative release of DOX could reach as high as about 69.5% within 60 h. These results undoubtedly demonstrated that the UCNPs/ZAIS drug delivery system has a strongly pH-dependent release of DOX. Additionally, instead of a burst release, the consecutive release situation was observed at the initial stage. This insteresting result indicate that the drug release is presumably managed by a diffusion-controlled release mechanism wherein the highly cross-linked polymer network plays a significant role.[36] This pH-dependent drug release could be exploited for controlled drug delivery applications.

We then incubated the HeLa cells with free DOX, UCNPs/ZAIS-FA and DOX-UCNPs/ZAIS-FA to demonstrate the cancer killing ability (Fig. 4d). It is obvious that without DOX, the HeLa cells had much higher viability than other samples. The half-maximum inhibitory concentration (IC50) for DOX-UCNPs/ZAIS-FA (6.3 μM) was found to be higher than that of free DOX (3.7 μM), this reduced toxicity is likely due to the slower release of DOX from DOX-UCNPs/ZAIS-FA.[37-40] Furthermore, high concentrations of DOX-UCNPs/ZAIS displayed higher cytotoxicity to cancer cells than free DOX, suggesting that DOX was more effectively transported into the cell by the UCNPs/ZAIS platform than when used alone. Therefore, it could be concluded that UCNPs/ZAIS have promising potential for drug loading and delivery in cancer therapy.

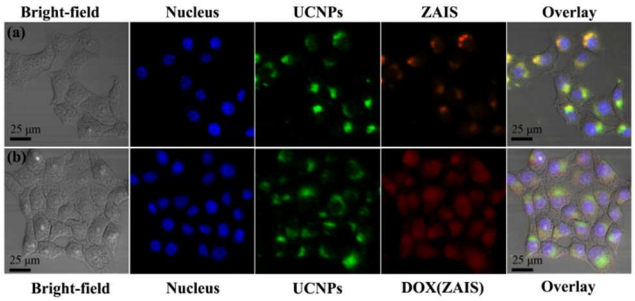

Fig. 5 CLSM images of HeLa cells incubated with (a) UCNPs/ZAIS-FA NCs, (b) DOX-UCNPs/ZAIS-FA for 1 h at 37 °C. The concentration of UCNPs/ZAIS-FA and DOX were 80 μg mL^{-1} and 20 μM, respectively.

As a proof of concept, the DC-UC multifunctional nanocomposites were used for dual-modal luminescence imaging on HeLa cells. The targeting molecule, FA, was covalently functionalized to the NCs *via* EDC/NHS binding. Then the UCNPs/ZAIS-FA NCs and DOX-UCNPs/ZAIS-FA were incubated with HeLa cells for confocal UC luminescence and DC fluorescence imaging. As shown in Fig. 5a, under 980 nm laser and 365 nm UV excitations, strong green UC luminescence signals at 550 nm (UCNPs) and yellow fluorescence at 650 nm (ZAIS) were observed respectively and showed obvious co-localization, demonstrating that the UCNPs and ZAIS were incorporated into the same NPs, which were rather stable inside cells. Meanwhile, the observed yellowish-green signal obtained by overlaying the yellow DC and green UC signals further established that the emission signals came from the same area stained with NCs. By contrast, after DOX loading, we observed bright UC signals and DOX fluorescence signals were evenly distributed inside cells owing to the intracellular release of DOX molecules from the samples. In addition, the DC emission of ZAIS was hard to distinguish because the emission of ZAIS overlapped with that of DOX (Fig. S4b). At last, it is clearly to see that almost every HeLa cell have bright signals, which could be ascribed to the highly specific interaction between FA and folate receptor on the HeLa cells.[40,41] For comparision, NCs without FA modification were used for control group (Fig. S6), where only a few weak DC and UC fluorescence signals were observed on the cells. Therefore, the results indicated that these as-prepared luminescence NCs could be used as multimodal biomarkers for biomedical labelling applications.

4. Conclusion

In summary, dual-modal luminescence NCs were successfully prepared through a facile strategy of aqueously cross-linking $NaYF_4$:Yb,Er UCNPs with ZAIS DC QDs. Carboxyl-functionalized β-$NaYF_4$:Yb,Er NPs were synthesized by one-pot solvothermal approach, which were convenient to cross-link with amino-modified ZAIS QDs. By take advantage of the original and distinct properties including DC and UC luminescence, these NCs are not only water-stable but also bioconjugatable with targeting biomolecules, facilitating their multifunctional bioapplications in DC-UC dual-modal luminescence imaging. Furthermore, utilizing a well-established folate targeting model, targeted selective DC-UC dual-modal luminescence imaging and drug delivery were achieved *in vitro*. Thus, these NCs could be used as potential biolabels for multi-modal imaging, and as promising drug carriers for intracellular drug delivery, suggesting the potentials a multifunctional nanoplatform for simultaneous diagnosis and therapy.

Acknowledgements

This work was supported by the National Natural Science Foundation of China (21471056, 21236003, 21206042, and 21176083), the Basic Research Program of Shanghai (13NM1400700, 13NM1400701), and the Fundamental Research Funds for the Central Universities.

References

a Key Laboratory for Ultrafine Materials of Ministry of Education, School of Materials Science and Engineering, East China University of

Science and Technology, Shanghai 200237, China. Fax: +86 21 6425 0624; Tel: +86 21 6425 2022; E-mail: yhzhu@ecust.edu.cn and czli@ecust.edu.cn
b The State Key Laboratory of Bioreactor Engineering, East China University of Science and Technology, Shanghai 200237, PR China
† Electronic Supplementary Information (ESI) available: additional Figures as noted in the text. See DOI: 10.1039/b000000x/

1 A. M. Smith and S. Nie, *Acc. Chem. Res.*, 2010, **43**, 190.
2 W. C. W. Chan and S. M. Nie, *Science*, 1998, **281**, 2016.
3 S. Zhuo, M. Shao, and S. Lee, *ACS Nano*, 2012, **6**, 1059.
4 M. D. Regulacio, K. Y. Win, S. L. Lo, S. Zhang, X. Zhang, S. Wang, M. Han and Y. Zheng, *Nanoscale*, 2013, **5**, 2322.
5 D. R. Baker and P. V. Kamat, *Adv. Funct. Mater.*, 2009, **19**, 805.
6 K. Shin, S. H. Im and J. H. Park, *Chem. Commun.*, 2010, **46**, 2385.
7 R. Vogel, P. Hoyer and H. Weller, *J. Phys. Chem.*, 1994, **98**, 3183.
8 T. L. Li and H. Teng, *J. Mater. Chem.*, 2010, **20**, 3656.
9 H. Na, K. Woo, K. Lim and H. S. Jang, *Nanoscale*, 2013, **5**, 4242.
10 Y. Dai, H. Xiao, J. Liu, Q. Yuan, P. Ma, D. Yang, C. Li, Z. Cheng, Z. Hou, P. Yang, and J. Lin, *J. Am. Chem. Soc.*, 2013, **135**, 18920.
11 J. C. Boyera and F. C. J. M. van Veggel, *Nanoscale*, 2010, **2**, 1417.
12 Z. Y. Hou, C. X. Li, P. A. Ma, Z. Y. Cheng, X. J. Li, X. Zhang, Y. L. Dai, D. M. Yang, H. Z. Lian and J. Lin, *Adv. Funct. Mater.*, 2012, **22**, 2713.
13 M. An, J. Cui, Q. He and L. Wang, *J. Mater. Chem. B*, 2013, **1**, 1333.
14 M. P. Melancon, M. Zhou and C. Li, *Acc. Chem. Res.*, 2011, **44**, 947.
15 Y. Dai, P. Ma, Z. Cheng, X. Kang, X. Zhang, Z. Hou, C. Li, D. Yang, X. Zhai, and J. Lin, *ACS Nano*, 2012, **6**, 3327.
16 L. Li, C. Liu, L. Zhang, T. Wang, H. Yu, C. Wang and Z. Su, *Nanoscale*, 2013, **5**, 2249.
17 L. Zhao, J. Peng, Q. Huang, C. Li, M. Chen, Y. Sun, Q. Lin, L. Zhu, and F. Li, *Adv. Funct. Mater.*, 2014, **24**, 363.
18 Y. Liu, D. Tu, H. Zhu, R. Li, W. Luo, and X. Chen, *Adv. Mater.*, 2010, **22**, 3266.
19 P. Li, Q. Peng, and Y. Li, *Adv. Mater.*, 2009, **21**, 1945.
20 P. Zhao, Y. Zhu, X. Yang, J. Shen, X. Jiang, J. Zong and C. Li, *Dalton Trans.*, 2014, **43**, 451.
21 P. Zhao,Y. Wu, Y. Zhu, X. Yang, X. Jiang, J. Xiao, Y. Zhang and C. Li, *Nanoscale*, 2014, **6**, 3804.
22 W. S. Zou, D. Sheng, X. Ge, J. Q. Qiao and H. Z. Lian, *Anal. Chem.*, 2011, **83**, 30.
23 M. Pedroni, F. Piccinelli, T. Passuello, M. Giarola, G. Mariotto, S. Polizzi, M. Bettinelli and A. Speqhini, *Nanoscale*, 2011, **3**, 1456.
24 A. Permadi, M. Z. Fahmi, J. K. Chen, J. Y. Chang, C. Y. Cheng, G. Q. Wang and K. L. Qu, *RSC Adv.*, 2012, **2**, 6018.
25 S. Gai, P. Yang, C. Li, W. Wang, Y. Dai, N. Niu, and J. Lin, *Adv. Funct. Mater.*, 2010, **20**, 1166.
26 A. A. Arnold, V. Terskikh, Q. Y. Li, R. Naccache, I. Marcotte, and J. A. Capobianco, *J. Phys. Chem. C*, 2013, **117**, 25733.
27 C. Li and J. Lin, *J. Mater. Chem.*, 2010, **20**, 6831.
28 H. Zhou, C. Xu, W. Sun, and C. Yan, *Adv. Funct. Mater.*, 2009, **19**, 3892.
29 M. Wang, C. C. Mi, W. X. Wang, C. H. Liu, Y. F. Wu, Z. R. Xu, C. B. Mao, and S. K. Xu, *ACS Nano*, 2009, **3**, 1580.
30 Q. Ju, D. Tu, Y. Liu, R. Li, H. Zhu, J. Chen, Z. Chen, M. Huang and X. Chen, *J. Am. Chem. Soc.*, 2012, **134**, 1323.
31 Z. Wang, J. Hao, H. L. W. Chan, W. Wong, and K. Wong, *Small*, 2012, **8**, 1863.
32 G. S. Yi and G. M. Chow, *Adv. Funct. Mater.,* 2006, **16**, 2324.
33 M. Langevin, A. M. Ritcey, and C. N. Allen, *ACS Nano*, 2014, **22**, 3476.
34 M. D. Regulacio, K. Y. Win, S. L. Lo, S. Zhang, X. Zhang, S. Wang, M. Han and Y. Zheng, *Nanoscale*, 2013, **5**, 2322.
35 C. Wang, L. Cheng, Z. Liu, *Biomaterials*, 2011, **32**, 1110.
36 W. Ma, K. Wu, J. Tang, D. Li, C. Wei, J. Guo, S. Wang and C. Wang, *J. Mater. Chem.*, 2012, **22**, 15206.
37 G. Tian, Z. Gu, L. Zhou, W. Yin, X. Liu, L. Yan, S. Jin, W. Ren, G. Xing, S. Li, and Y. Zhao, *Adv. Mater.*, 2012, **24**, 1226.
38 D. Yang, Y. Dai, J. Liu, Y. Zhou, Y. Chen, C. Li, P. Ma, J. Lin, *Biomaterials*, 2014, **35**, 2011.
39 G. Tian, W. Yin, J. Jin, X. Zhang, G. Xing, S. Li, Z. Gu, and Y. Zhao, *J. Mater. Chem. B*, 2014, **2**, 1379.
40 P. S. Xu, E. A. Van Kirk, Y. H. Zhan, W. J. Murdoch, M. Radosz and Y. Q. Shen, *Angew. Chem., Int. Ed.*, 2007, **46**, 4999.
41 R. Naccache, P. Chevallier, J. Lagueux, Y. Gossuin, S. Laurent, L. V. Elst, C. Chilian, J. A. Capobianco, and M. Fortin, *Adv. Healthc. Mater.*, 2013, **2**, 1478.

Graphical Abstract

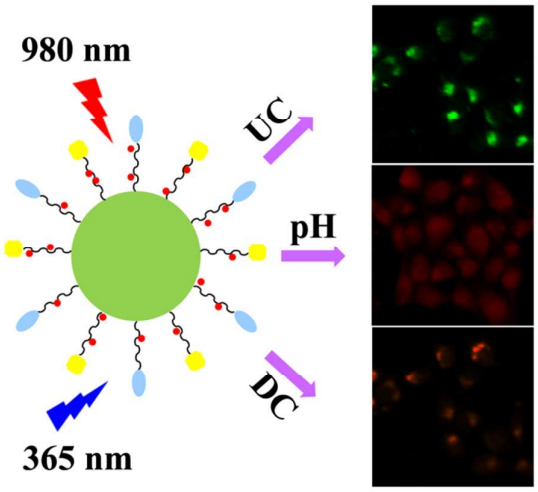

A highly efficient multifunctional nanoplatform for dual-modal luminescence imaging and pH-responsive drug delivery has been developed on the basis of a facile and novel strategy by covalently binding up-conversion luminescence $NaYF_4$:Yb,Er nanoparticles with down-conversion fluorescence $AgInS_2$-ZnS quantum dots.